Nonlinear field effects in quadrupole mass filters

J. Schulte,[a] P. V. Shevchenko,[b] and A. V. Radchik[c]
Department of Applied Physics, University of Technology, NSW 2007, Sydney, Australia

(Received 4 December 1998; accepted for publication 25 May 1999)

The performance of a quadrupole mass filter (QMF) generally degrades when using electrodes of circular cross section in place of mathematical ideal hyperbolic electrodes. The circular cross section of electrodes produces nonlinear resonances resulting in distortion and peak splitting in mass spectra. In addition, resonances reduce the actual working cross section, resulting in limited ion yield. In this article we study nonlinear resonances and intensities of resonance lines passing through the tip of the stability diagram of the QMF. We have found that balancing of multipole terms, rather than eliminating individual multipole terms, improves the sensitivity of the QMF considerably. The theory for assessing intensities of nonlinear resonances is presented in detail along with rescaling laws to adjust current QMF parameter settings. A general formula is presented from which the location and intensity of nonlinear can be derived, which then may be used for the design of special purpose QMFs. © *1999 American Institute of Physics.* [S0034-6748(99)01609-3]

INTRODUCTION

The quadrupole mass filter (QMF) most commonly employed in mass spectrometry was first described by Paul *et al.*[1] Though hyperbolic electrodes produce a perfect quadrupole field, in practice rods of circular cross section are being used for they are much easier to fabricate and to align (Fig. 1). The QMF is operated by applying dc and rf potentials to opposite electrodes in such that a low energy beam of ions from a source may pass through the length of the device if they meet certain charge and mass criteria. In a perfect quadrupole field the potential is then

$$\Phi(x,y,t)=(U-V\cos\omega t)\cdot \mathrm{Re}\{A_2 z^2\}, \quad z=x+iy, \quad (1)$$

which, of course, can be achieved by using hyperbolic electrodes. In such case the stability of ion motion depends on only two parameters, i.e., $a=8eU/(m\omega^2 r_0^2)$ and $q=8eU/(m\omega^2 r_0^2)$, respectively, where $r_0=R-r$ (see Fig. 1 for geometry definitions, all lengths are scaled to the unit radius of the casing). An (a,q) plane representation of stability lines, the so called stability diagram for mass separation, is shown in Fig. 2.

The potential field in the QMF with circular electrodes can be written as

$$\Phi(x,y,t)=(U-V\cos\omega t)\cdot \mathrm{Re}\{A_2 z^2+A_6 z^6+A_{10} z^{10} +\ldots\}, \quad z=x+iy, \quad (2)$$

where x and y are Cartesian coordinates, U and V are amplitudes of applied dc and ac voltages, respectively, and ω is the operating frequency. Due to the symmetry of the QMF, the nonlinear terms contributing to the field are of order z^{4n+2}. It has become common practice to choose the QMF design parameters such that the field term $A_6 z^6$ becomes zero, leaving only apparently weak nonlinear contributions of $A_{10}z^{10}$ and higher order field terms. The design parameters are usually expressed in terms of the ''magic number'' $\eta=r/(R-r)$ and a value of $\eta_1=1.1451$ has been established for the case of $A_6=0$.[2]

In previous studies,[2,3] it has been noted that within the region between electrodes and grounding case the affect of the grounding case on potential, Eq. (2), is negligibly small. Using a semianalytical approach[2] we found that in this region the potential between the electrodes may be considered independent of the radius of the grounding case with an uncertainty of up to 0.05%. Thus we may assume that only two length parameters r and R exist and all lengths can be rescaled with respect to R. Specific scaling rules for the multipole expansion coefficients A_i in Eq. (1) were then formulated. The scaling rules establish an analytic relationship between $\tilde{A}_i$ and r/R (Fig. 3) from which all coefficients $A_i(R,r)$ can be calculated for any r,R, i.e.,

$$A_i(r,R)\cdot R^i=\tilde{A}_i(r/R). \quad (3)$$

The scaling rules, Eq. (2), thus provide the QMF operating parameters with an accuracy of up to 0.05%. Employing Eq. (3) we calculated the following magic numbers: $\eta_1=1.1451$ for $A_6=0$, $\eta_2=0.760$ for $A_{10}=0$, and $\eta_3=0.591$ for $A_{14}=0$, respectively. It was found in Refs. 4–7 that the deviations from an ideal quadropole field cause nonlinear resonances which can broaden the tip region of the stability diagram significantly and thus may limit the resolution of the mass spectrometer as well as distort the shape of the output spectrum. In practice, the magic number η_1 which sets $A_6=0$ is used under the assumption that the term $A_{10}z^{10}$ is negligibly small such that it does not change the quadrupolarity of the field. The contribution of the $A_{10}z^{10}$ term on the resonance structure of the device, however, is not well known or discussed in the literature. We estimated that the contribution of the $A_{10}z^{10}$ term to the total potential is on the

[a]Electronic mail: jschulte@phys.uts.edu.au
[b]Present address: School of Physics, The University of New South Wales, Sydney, 2052, Australia.
[c]Present address: FuCell, The University of New South Wales, Sydney, 2052, Australia.

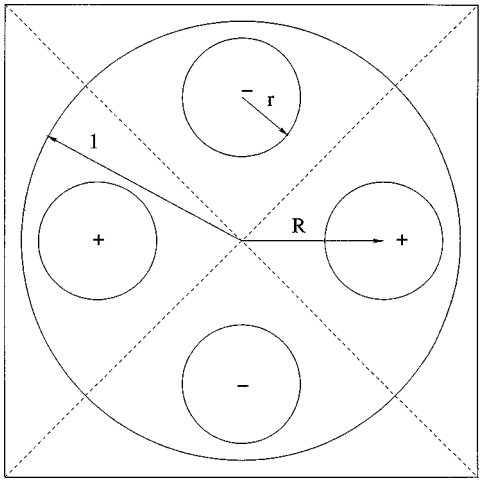

FIG. 1. Cross section of a conventional quadrupole mass filter with electrodes of circular cross section.

order of 10^{-3} in the case of $A_6=0$. With a deviation of the magic number η_1 by 1%, the contribution by the A_6z^6 term becomes of the same order of magnitude as the one expected by the $A_{10}z^{10}$ term, i.e., 10^{-3}. The corresponding shift in operating voltage is less than 1% and of little practical concern. The sensitivity of the QMF, however, is of real practical importance. It was already noticed by Denison[3] that the sensitivity, i.e., the available QMF cross section (ACS) is very sensitive to even small changes in r/R. Denison has estimated the ACS beyond which an ion cannot penetrate the QMF without colliding with an electrode to be only 45% of the total available cross section in the case of a resolution of 400 and the magic number $\eta=1.16$ established in Ref. 8. Also, he estimated that for a magic number of $\eta=1.1468$, established in Ref. 3, the ACS could be increased by 42% compared to a design with $\eta=1.16$. The reduction in available cross section is due to nonlinear resonances passing through the tip of the stability diagram. Taking into account the influence of resonances may thus be more important than merely eliminating the A_6z^6 term. We found that due to the nonlinear resonances the tip in the stability diagram is broadened by about $\delta\beta_x\approx 1/\xi_{\max}\approx 0.005$ ($\xi_{\max}\approx 200$, the standard value of the time needed to pass through the QMF taken from Ref. 9) and hence the tip of the diagram can no longer be regarded as a single intercept point any more (Fig. 4). In practical terms, for operating lines corresponding to mass resolutions of $m/\delta m\sim 1/\delta\beta_x\sim 200+$, ions will always be affected by nonlinear resonances.

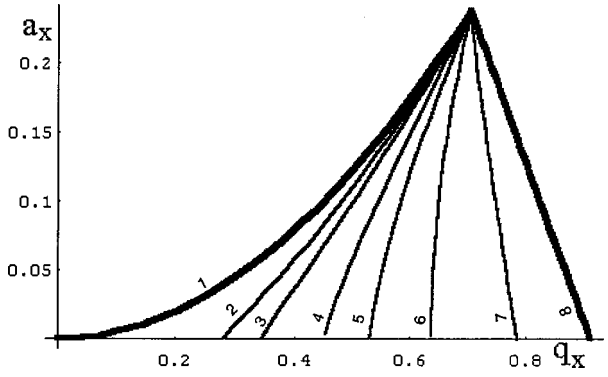

FIG. 2. Stability diagram and resonance lines: (2) $\beta_x\pm 4\beta_y=1$, (3) $\beta_x\pm 3\beta_y=1$, (4) $\beta_x\pm 2\beta_y=1$, (5) $\beta_x\pm 3/2\beta_y=1$, (6) $\beta_x\pm\beta_y=1$, (7) $\beta_x\pm\beta_y/2=1$. Lines (1) and (8) correspond to $\beta_y=0$ and $\beta_x=1$, respectively, and form the border lines of the stability diagram. The tip position is $q_x=0.706$, $a_x=0.237$.

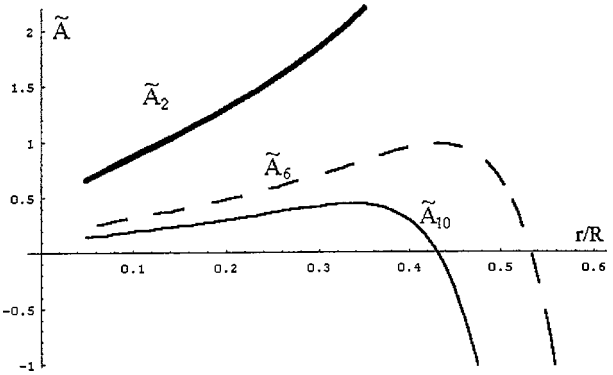

FIG. 3. Multipole coefficients $\tilde{A}_i$ vs r/R. The solutions of $\tilde{A}_i(r/R)=0$ yield corresponding magic numbers $\eta_i=r/(r-R)$.

NONLINEAR RESONANCES AND THEIR RELATIONSHIP TO MULTIPOLE FIELDS IN QMF

In order to assess the significance of the nonlinear resonance contributions, we analyzed the strongest resonance lines due to the A_6z^6 and $A_{10}z^{10}$ terms which are passing through the tip of the stability diagram, i.e., the region where the QMF is being operated in practice.

The Hamiltonian of the system under consideration is

$$H(p_x,p_y,x,y,t)=\frac{p_x^2}{2m}+\frac{p_y^2}{2m}+e\cdot\Phi(x,y,t), \tag{4}$$

where m and e are the mass and the charge of the ion, respectively, and P_x and P_y are the ion momenta. After introducing quardupole parameters

$$a_x=-a_y=\frac{8eU}{m\omega^2}A_2,\quad q_x=-q_y=\frac{4eV}{m\omega^2}A_2,\quad \xi=\frac{\omega t}{2}, \tag{5}$$

where a_x and q_x are the usual trap parameters multiplied by A_2, the equation of motion for ions is then

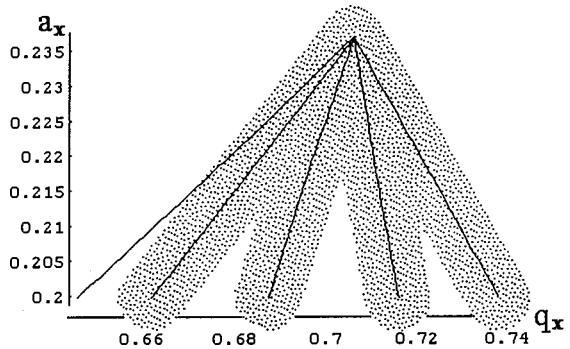

FIG. 4. The cropped tip of the stability diagram is a broad spot due to cumulation of nonlinear resonances, illustrated by a gray shaded area (see text) shown here for lines with $\beta_x+2\beta_y=1$, $\beta_x+\beta_y=1$, $\beta_x+\beta_y/2=1$, and $\beta_x=1$, respectively.

$$\ddot{x}+(a_x-2q_x\cos 2\xi)\cdot x=-\frac{\partial h'}{\partial x},$$
$$\ddot{y}+(a_y-2q_y\cos 2\xi)\cdot y=-\frac{\partial h'}{\partial y}. \tag{6}$$

The corresponding Hamiltonian function is

$$h(p_x,p_y,x,y,\xi)=h_0(p_x,p_y,x,y,\xi)+h'(x,y,\xi), \tag{7}$$

with

$$h_0=\tfrac{1}{2}[p_x^2+(a_x-2q_x\cos 2\xi)x^2+p_y^2+(a_y-2q_y\cos 2\xi)y^2],$$
$$h'(x,y,\xi)=\frac{1}{2}(a_x-2q_x\cos 2\xi)\cdot\left(\frac{A_6}{A_2}\mathrm{Re}\{z^6\}+\frac{A_{10}}{A_2}\mathrm{Re}\{z^{10}\}+\ldots\right).$$

The linear approximation of the equation of motion, Eq. (6), leads to the well known Mathieu equations for ideal hyperbolic electrodes. Here we consider the commonly used stability region (Fig. 2), where the ions are stable in linear approximation. We note that the Hamiltonian h has a period of π with respect to the dimensionless time ξ. The canonical matrix transformation[8] $\mathbf{X}=\hat{B}\boldsymbol{\zeta}$

$$\begin{pmatrix} x\\ p_x\\ y\\ p_y\end{pmatrix}=\hat{B}\cdot\begin{pmatrix}\zeta_1\\ \zeta_2\\ \zeta_3\\ \zeta_4\end{pmatrix} \tag{8}$$

transforms the time-dependent Hamiltonian h_0 to the time-independent form

$$\tilde{h}_0(\boldsymbol{\zeta})=\beta_x(\zeta_1^2+\zeta_2^2)/2+\beta_y(\zeta_3^2+\zeta_4^2)/2. \tag{9}$$

The corresponding equations of motion are then

$$\ddot{\zeta}_1+\beta_x^2\zeta_1=0,\quad \zeta_2=\dot{\zeta}_1/\beta_x,$$
$$\ddot{\zeta}_3+\beta_y^2\zeta_3=0,\quad \zeta_4=\dot{\zeta}_3/\beta y. \tag{10}$$

The matrix elements of $\hat{B}$ are

$$\hat{B}=\begin{pmatrix} B_{11}^x & B_{12}^x & 0 & 0\\ B_{21}^x & B_{22}^x & 0 & 0\\ 0 & 0 & B_{11}^y & B_{12}^y\\ 0 & 0 & B_{21}^y & B_{22}^y\end{pmatrix}, \tag{11}$$

with

$$B_{11}^i=1/2\sum_n C_{2n}^i\cdot\cos 2n\xi,\quad B_{12}^i=1/2\sum_n C_{2n}^i\cdot\sin 2n\xi,$$
$$B_{21}^i=-1/2\sum_n C_{2n}^i\cdot(2n+\beta_i)\cdot\sin 2n\xi, \tag{12}$$
$$B_{22}^i=1/2\sum_n C_{2n}^i\cdot(2n+\beta_i)\cdot\cos 2n\xi,\quad i=x,y.$$

Here β_i, C_{2n}^i are parameters of the Mathieu functions, which can be calculating to an arbitrary accuracy by means of the familiar recurrent equations presented in Ref. 9. Since the sums in Eq. (12) converge very rapidly ($C_{\pm 4}^i/C_{\pm 2}^i\approx 10^{-2}$) we shall only consider terms including C_i^o and $C_{\pm 2}^i$. It is worthwhile to note that the periodic transformation $\hat{B}$ leaves the stability properties in the new and old variables unchanged. The transformed total nonlinear Hamiltonian is

$$K(\boldsymbol{\zeta},\xi)=\tilde{h}_0+h'(\hat{B}\boldsymbol{\zeta},\xi). \tag{13}$$

The new Hamiltonian function under the canonical transformation, Eq. (8), relates to the one in Eq. (7) through

$$K(\boldsymbol{\zeta},\xi)=h(x,p_x,y,p_y,\xi)+\frac{\partial F(\zeta_2,x,\zeta_4,y,\xi)}{\partial\xi}, \tag{14}$$

where $F(\zeta_2,x,\zeta_4,y,\xi)$ is the generating function satisfying

$$\zeta_1=\frac{\partial F}{\partial\zeta_2},\quad \zeta_3=\frac{\partial F}{\partial\zeta_4},\quad p_x=\frac{\partial F}{\partial x},\quad p_y=\frac{\partial F}{\partial y}. \tag{15}$$

With Eqs. (8), (12), and (15) the generating function $F(\zeta_2,x,\zeta_4,y,\xi)$ becomes

$$F=\frac{1}{2B_{11}^x}(B_{21}^x x^2+2\zeta_2 x-B_{12}^x\zeta_2^2)+\frac{1}{2B_{11}^y}(B_{21}^y y^2+2\zeta_4 y-B_{12}^y\zeta_4^2), \tag{16}$$

where F is a quadratic function based on the linearity of the transformation $\hat{B}$ and does not contribute to $h'(\hat{B}\boldsymbol{\zeta},\xi)$. Note that the order of nonlinear terms as well the period π of the Hamiltonian have been conserved.

We define $\langle dh/d\xi\rangle$ as the intensity of the nonlinear resonance, where $\langle\ldots\rangle$ represents the time average. Following the Hamiltonian formalism[10] we may write

$$\frac{dh}{d\xi}=\frac{\partial h}{\partial\xi}, \tag{17}$$

and thus find for the partial differentiation of Eq. (14) with respect to ξ

$$\frac{\partial h}{\partial\xi}=\frac{\partial K}{\partial\xi}-\frac{\partial^2 F}{\partial\xi^2}. \tag{18}$$

The term $^{\partial 2}F/^{\partial}\xi^2$ generates only quadratic corrections to total Hamiltonian while the perturbation $h'(\hat{B}\boldsymbol{\zeta},\xi)$ is of order z^6 and higher. Therefore $^{\partial 2}F/^{\partial}\xi^2$ cannot produce new resonance lines inside the first stability region and we may consider the time average of this term to be zero. With Eqs. (13), (17), and (18) we can derive the intensity of the nonlinear resonance

$$\left\langle\frac{dh}{d\xi}\right\rangle=\left\langle\frac{\partial h'(\hat{B}\boldsymbol{\zeta},\xi)}{\partial\xi}\right\rangle. \tag{19}$$

The intensity is nonzero only along the resonance lines. If we take the first order approximation of the system of nonlinear equations (6), we obtain the following solutions for Eq. (10):

TABLE I. Intensities $\langle dh/d\xi \rangle$ of the resonance lines $\beta_x + k \cdot \beta_y = 1$ when working with device parameters set to match the tip of stability diagram ($q_x = 0.706$, $a_x = 0.237$).

$$\left\langle \frac{dh}{d\xi} \right\rangle = \frac{A_i}{A_2} \frac{a^n b^{i-n}}{2^{i+1}} \sin \gamma \cdot \alpha_i, \quad i = 6,10$$

$i=6$													
k	0	0	0	0	0	1	1	−2	−1	1/2	−1/2	2	−1
n	4	4	6	2	6	4	2	2	2	4	4	2	4
γ	$4c$	$2c$	$2c$	$2c$	$4c$	$2c+2d$	$2c+2d$	$2c-4d$	$2c-2d$	$4c+2d$	$4c-2d$	$2c+4d$	$2c-2d$
α_6	−9.6	10.3	1.3	−0.38	−1.6	4.8	−3.6	−0.95	−3.76	−4.0	−3.7	−0.95	5.0
$i=10$													
k	0	0	0	0	0	0	0	0	0	1/2	−1/2	3	3/2
n	8	4	6	6	2	8	10	10	4	6	6	4	4
γ	$4c$	$4c$	$2c$	$4c$	$2c$	$2c$	$4c$	$2c$	$2c$	$4c+2d$	$4c-2d$	$2c+6d$	$4c+6d$
α_{10}	−81	−69	−112	184	−10.6	37	4.8	−1.8	80	100	95	4.0	−3.0
k	−2	−2	−3	4	3	2	1/2	1	1	−1/2	−1	−1	−3	−2
n	4	6	4	2	2	2	8	2	8	8	2	8	2	2
γ	$2c-4d$	$2c-4d$	$2c-6d$	$2c+8d$	$2c+6d$	$2c+4d$	$4c+2d$	$2c+2d$	$2c+2d$	$4c-2d$	$2c-2d$	$2c-2d$	$2c-6d$	$2c-4d$
α_{10}	23	−18.5	3.7	−0.15	−1.2	−4.2	−32	−7.5	17	−30	−8.3	18	−1.15	−4.2

$$\eta_1 = a \cos(\beta_x \xi + c), \quad \eta_2 = -a \sin(\beta_x \xi + c),$$
$$\eta_3 = b \cos(\beta_y \xi + d), \quad \eta_4 = -b \sin(\beta_y \xi + d), \tag{20}$$

where a,b are initial amplitudes and c,d respective phases. Equation (19) can now be solved with Eq. (20) and resonance lines and corresponding intensities can be obtained.

RESONANCE INTENSITIES

According to Wang *et al.*[6] all resonance lines are expected to satisfy the general condition

$$\beta_x n_1 + \beta_y n_2 = 2\nu, \tag{21}$$

where n_1, n_2, and ν are integers. In the following we restrict our consideration to resonance lines passing through the tip of the stability diagram ($n_1 = 2\nu$), i.e., to lines which affect the accuracy of the QMF most (Figs. 2 and 4). From the solution of Eq. (20) we found that nonlinearity of order $\mathrm{Re}(z^6)$ produces the following resonance lines (i.e., those passing through the tip of the stability diagram).

$$\beta_x = 1, \quad \beta_x + 2\beta_y = 1, \quad \beta_x + \beta_y/2 = 1, \quad \beta_x + \beta_y = 1,$$
$$\beta_x - 2\beta_y = 1, \quad \beta_x - \beta_y = 1, \quad \beta_x - \beta_y/2 = 1. \tag{22}$$

The nonlinearity of order $\mathrm{Re}(z^{10})$ yields resonance lines for

$$\beta_x = 1, \quad \beta_x + \beta_y = 1, \quad \beta_x + \beta_y/2 = 1, \quad \beta_x + 2\beta_y = 1,$$
$$\beta_x + 3\beta_y = 1, \quad \beta_x + 4\beta_y = 1, \quad \beta_x + 3/2\beta_y = 1,$$
$$\beta_x - 4\beta_y = 1, \quad \beta_x - 3\beta_y = 1, \quad \beta_x - 2\beta_y = 1, \tag{23}$$
$$\beta_x - \beta_y = 1, \quad \beta_x - \beta_y/2 = 1, \quad \beta_x - 3/2\beta_y = 1.$$

The intensities of resonance lines are then

$$\left\langle \frac{dh}{d\xi} \right\rangle = \frac{A_i}{A_2} \frac{a^{n_k} b^{i-n_k}}{2^{i+1}} \sin \gamma \cdot \alpha_i, \quad i = 6,10. \tag{24}$$

Each line k is characterized by a set of parameters γ, n_k, and α_i, respectively. The resonance intensity factor α_i is a function of the position along the resonance line. In Table I. α_i are presented for QMF parameters representing the tip of the stability diagram ($q_x = 0.706$, $a_x = 0.237$) as well as for the nonlinear resonances of Eqs. (22) and (23). From Table I it becomes obvious that the strongest lines are not necessarily subject to the condition $|n_1| + |n_2| = N$ (where N is the order of nonlinearity, and $\nu = 1$) as reported in the literature.[6,7] Instead we found that the strongest lines in descending order of intensity are actually

$$\beta_x = 1, \quad \beta_x + \beta_y = 1, \quad \beta_x + \beta_y/2 = 1, \quad \beta_x + 2\beta_y = 1. \tag{25}$$

These lines satisfy condition (21), however, they do not satisfy the condition $|n_1| + |n_2| = N$ reported in Refs. 6 and 7. This result has further implications on design parameters and will be discussed in the following section.

THE RESONANCE STRUCTURE AND CORRECTION TO THE MAGIC NUMBER

The magic number η_1 is usually obtained for the condition $A_6 = 0$ and under the assumption that the field contribution by $A_{10} z^{10}$ is negligible small.[3,8] We found that the negligibility of $A_{10} z^{10}$ is valid for all points within the stability diagram except for the nonlinear resonance lines. Our calculations have lead us to the conclusion that the elimination of coefficient A_6 produces considerable nonlinear contributions and, therefore, a field configuration where A_6, $A_{10} \neq 0$, such that $A_6 z^6$ and $A_{10} z^{10}$ are balancing each other so as to decrease the loss of ions due to resonances, may result in better performance. In order to estimate the required corrections to η_1 to satisfy the new balancing condition, we calculated the corrections to Eq. (20) (second harmonics). The corrections are proportional to time and to the intensity of the resonance line, which in turn is proportional to the multipole coefficient A_i of the potential expansion. We worked within the framework of the conventional perturbation theory where the second harmonics is considered smaller than the first one.

With the analytical expression for nonlinear contributions to the intensity derived so far, we are now in the posi

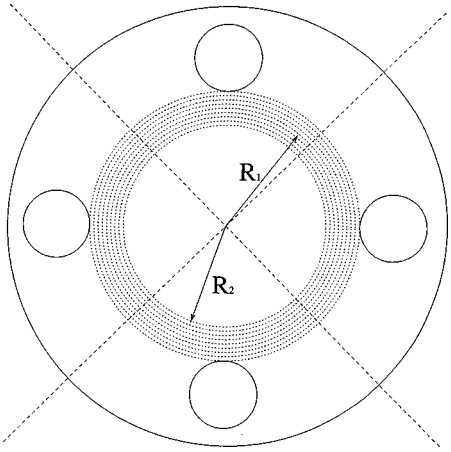

FIG. 5. Available cross section (see text). Ions within the white inner circular area are stable, if they are stable within linear approximation. Ions in the dashed area will be lost due to nonlinear resonances.

tion to optimize the ACS of the device. Here we make the assumption that the ion entry displacement R_0 from the axis along the center of the device is such that $R_0 < r_0$. In linear approximation we then have a stable ion trajectory which then passes through the QMF device. But in practice the influence of the nonlinear resonances leads to an increase of the second harmonics in the radial displacement of ions causing loss of ions that otherwise would have stable trajectories.

Therefore in the presence of resonances a critical radius R_{crit} should exist such that for a stable ion trajectory we find $R_0 < R_{\text{crit}} < r_0$. Let us consider two forms of the electrical potential in the QMF:

$$\Phi_1 = A_2 z^2 + A_{10} z^{10}, \quad \Phi_2 = A_2 z^2 + A_6 z^6 \tag{26}$$

for which the corresponding magic numbers are $\eta_1 = 1.1451$ (satisfying $A_6 = 0$) and $\eta_2 = 0.760$ (satisfying $A_{10} = 0$). For both potentials we can introduce different values of critical radii: R_1 and R_2, respectively, see Fig. 5 (Fig. 5 is for illustration only, in reality R_{crit} is a function of the polar angle which, in general, will not produce a circular shaped ACS). We found that the maximum ion yield (i.e., minimum ion loss due to resonances) can be achieved by appropriate balancing of the $A_6 z^6$ and $A_{10} z^{10}$ terms. Assuming that initial ion velocities are zero and the ion density is constant over the cross section of the device,[9] we can introduce the normalized ion loss P_n as an integral over the ''dashed ring'' region in Fig. 5 (the region where $R_{\text{crit}} < R_0 < r_0$)

$$P_n = \frac{1}{N} \int_{R_{\text{crit}}}^{r_0} dx_0 \, dy_0, \tag{27}$$

where $N = \pi r_0^2$, and x_0 and y_0 are the initial ion displacements. Since at the tip of the stability diagram we have $\beta_y \to 0$, an increase of ion amplitude due to resonances will occur only in the x direction. In this case, from Eq. (26) we can derive the following expression:

$$P_n \propto \frac{r_0^8}{R^8} \int_0^1 d\rho \cdot \sqrt{1-\rho^2} \left(\frac{\tilde{A}_6\left(\frac{r}{R}\right)}{\tilde{A}_2\left(\frac{r}{R}\right)} \sum_k \alpha_{6_k} (1-\rho^2)^{(n_k/2)-1} \times \rho^{6-n_k} + \frac{\tilde{A}_{10}\left(\frac{r}{R}\right)}{\tilde{A}_2\left(\frac{r}{R}\right)} \cdot \left[1 - \frac{r}{R}\right]^4 \times \sum_k \alpha_{10_k} (1-\rho^2)^{(n_k/2)-1} \rho^{10-n_k} \right), \tag{28}$$

where α_6, α_{10}, and n_k correspond to resonance lines with index k, see Table I. A derivation of Eq. (28) is given in the Appendix. Using the data from Table I we found P_{min} (minimum ion loss) for $r/R = 0.523$. The corresponding new magic number is $\eta_s = 1.10$. Comparing the ion loss P_{min} of this design, i.e., $\eta_s = 1.10$, and the ion loss P_0 of the traditional setting, $\eta_1 = 1.1451$, we found a ratio of ion losses of $P_{\text{min}}/P_0 \approx 0.6$. Thus, with a QMF design which balances the $A_6 z^6$ and $A_{10} z^{10}$ multipole terms, i.e., with $\eta_s = 1.10$, a further substantial improvement in QMF sensitivity ($\approx 40\%$) can be achieved.

RESULTS AND DISCUSSION

Our result not only emphasises that a considerable increase in ion yield can be achieved by proper design parameter adjustments, it also shows that tuning the magic number to eliminate one individual multipole term does not provide operational improvements of technological significance. Our suggested approach may thus result in superior device performance. It is worthwhile to mention that Eq. (28) can also be used to derive design parameters which will decrease the affect of some specific resonances in the tip, thus providing the means to construct or improve a special purpose QMF. In the following, we present the new scaling rules which will allow the adjustment of current designs.

The definition of the stability parameters of the ideal hyperbolic potential given by[9]

$$a_x' = -a_y' = \frac{8eU}{m\omega^2 r_0^2}, \quad q_x' = -q_y' = \frac{4eV}{m\omega^2 r_0^2}, \tag{29}$$

can be transformed to our definition in Eq. (5) by setting $A_2 = 1/r_0^2$. This enables us to formulate the rescaling relations

$$a_x / a_x' = q_x / q_x' = A_2 r_0^2 = \tilde{A}_2(r/R) \cdot (1 - r/R)^2 = \kappa(r/R). \tag{30}$$

The rescaling coefficient κ depends only on the magnitude of the magic number $\eta = r/(R-r)$. For our new magic number ($\eta_s = 1.10$) we found $\kappa = 0.999$. Note that our magic number is much different from the one ($\eta_1 = 1.1451$, $\kappa = 1.0028$) commonly referenced.

In summary, we have found that the boundaries of the stability diagram are narrow stripes rather than perfect lines and that the tip of the diagram is a broad spot rather than a single intercept point. The broadening of the boundaries of the stability diagram is caused by the cumulation of nonlinear resonances (Fig. 4). The width of the individual resonance lines is about $\delta\beta_x \approx 1/\xi_{\max} \approx 0.005$ ($\xi_{\max} \approx 200$, standard value taken from Ref. 9). Our results show that a considerable improvement in mass detection can be achieved by balancing the multipole terms to decrease nonlinear resonance effects. This approach is much different from the current practice of shifting the QMF operating line somewhat below the broadened tip point. Ions which are close to the stability tip are always influenced by resonances and only due to the finite length of the QMF are passing through the device. Proper balancing of the multipole terms is required to increase ion yield, i.e., the overall sensitivity of the QMF.

ACKNOWLEDGMENTS

This work has been supported in part by Balzers Instruments Ltd. (Liechtenstein) and UTS Industry Link Grant 1998.

APPENDIX

Since in the tip of the stability diagram we have $\beta_y \rightarrow 0$, an increase of ion amplitude due to resonances will occur only in the x direction. To a first order approximation, the correction $\delta\zeta_1$ to Eq. (20) in the transformed coordinate system is

$$\delta\ddot{\zeta}_1 + \beta_x^2 \delta\zeta_1 = -\frac{\partial h'(\hat{B}\boldsymbol{\zeta}, \xi)}{\partial \zeta_1}. \tag{A1}$$

In the following, for simplicity, we consider only a single arbitrary resonance term. The right hand side of Eq. (A1) can then be written $Q\cos(\beta_x\xi + \delta)$, where $Q \sim a^{n-1}b^{i-n}$ ($i = 6,10$, i.e., the order of nonlinearity) and δ is a linear function of initial phases c and d, respectively. In this case we find that $\delta\zeta_1 = \frac{1}{2}Q\xi\sin(\xi+\delta)$. Hereafter we set $\beta_x = 1$, $\beta_y = 0$ which corresponds to the tip of the stability diagram. The Hamiltonian of Eq. (A1) is then

$$K = \tfrac{1}{2}(\zeta_1^2 + \zeta_2^2) - Q\cos(\xi+\delta)\zeta_1. \tag{A2}$$

The intensity of the resonance is $\langle dh/d\xi\rangle = \langle \partial K/\partial\xi\rangle = \frac{1}{2}Qa\sin\gamma$. Comparing this intensity with Eq. (24) we can now calculate the amplitude of correction $\delta\zeta_1$ due to one resonance term

$$\Lambda^{(2)} = \frac{1}{2}Q\cdot\xi = \xi\frac{A_i}{A_2}\frac{\alpha_i}{2^{i+1}}a^{n-1}b^{i-n}, \tag{A3}$$

where n, α_1, and i are the parameters of the resonance line. The amplitude $\Lambda^{(2)}$ due to all resonance terms can be found by integrating over all resonance lines in Eq. (A3). Using the linear transformation, Eq. (7), we find the initial amplitudes in the xy space are $x_0 \approx \frac{1}{2}a$, $y_0 \approx \frac{1}{2}b$, and maximum displacements in xy space are $x_{\max} \approx x_0 + (a/4)(\Lambda^{(2)}/a)^2$, $y_{\max} \approx y_0$. In order to find the critical initial displacement $x_0 = x_{\text{crit}}$ in the x direction for a given y_0, we solve $x_{\max} = \sqrt{r_0^2 - y_0^2}$ (ions with initial displacements of $x_0 > x_{\text{crit}}$ will be lost). Since $|\Lambda^{(2)}| \ll a$, we find $x_{\text{crit}} \approx \sqrt{r_0^2 - y_0^2} - (a/4)(\Lambda^{(2)}/a)^2$ (here we substitute $a \approx 2\sqrt{r_0^2 - y_0^2}$ and $b \approx 2y_0$). Now we can calculate the normalized ion loss, Eq. (27)

$$\begin{aligned}
P_n &= \frac{4}{\pi r_0^2}\int_0^{r_0} dy_0 \int_{x_{\text{crit}}}^{\sqrt{r_0^2 - y_0^2}} dx_0 \\
&\approx \frac{1}{\pi r_0}\int_0^1 a\left(\frac{\Lambda^{(2)}}{a}\right)^2 dy \\
&= \frac{\xi^2}{32\pi}\frac{r_0^8}{R^8}\int_0^1 d\rho\cdot\sqrt{1-\rho^2}\left(\frac{\tilde{A}_6\left(\frac{r}{R}\right)}{\tilde{A}_2\left(\frac{r}{R}\right)}\sum_k \alpha_{6_k}\right. \\
&\quad \times(1-\rho^2)^{n_k/2-1}\rho^{6-n_k} + \frac{\tilde{A}_{10}\left(\frac{r}{R}\right)}{\tilde{A}_2\left(\frac{r}{R}\right)} \\
&\quad \left.\cdot\left[1-\frac{r}{R}\right]^4\sum_k \alpha_{10_k}(1-\rho^2)^{(n_k/2)-1}\rho^{10-n_k}\right)^2,
\end{aligned} \tag{A4}$$

where the parameters α_6, α_{10}, and n_k correspond to the respective resonance lines with index k.

[1] W. Paul and H. Steinwedel, Z. Naturforsch. A **8**, 448 (1953).
[2] A. J. Reuben, A. V. Radchik, G. B. Smith, and A. V. Vagov, Rapid Commun. Mass Spectrom. **8**, 939 (1994).
[3] D. R. Denison, J. Vac. Sci. Technol. **8**, 266 (1971).
[4] F. von Busch and W. Paul, Z. Phys. **164**, 588 (1961).
[5] P. H. Dawson and N. R. Whetten, Int. J. Mass Spectrom. Ion Phys. **2**, 45 (1969); **3**, 1 (1969).
[6] Y. Wang, J. Franzen, and K. P. Wanczek, Int. J. Mass Spectrom. Ion Processes **124**, 125 (1992).
[7] Y. Wang, Rapid Commun. Mass Spectrom. **7**, 920 (1993).
[8] I. E. Dayton, F. C. Shoemaker, and R. F. Mozley, Rev. Sci. Instrum. **25**, 485 (1954).
[9] R. E. March and R. J. Hughes, *Quadrupole Storage Mass Spectrometry* (Wiley, New York, 1989), p. 31ff.
[10] L. D. Landau and E. M. Lifshitz, *Mechanics*, 3rd ed., Course of Theoretical Physics, Vol. 1 (Pergamon, Oxford, 1976), p. 94ff.